Picosecond near-to-mid-infrared absorption of pulse-injected small polarons in magnesium doped lithium niobate

FELIX FREYTAG,[1] **PHILLIP BOOKER,**[2] **GÁBOR CORRADI,**[3] **SIMON MESSERSCHMIDT,**[1] **ANDREAS KRAMPF,**[1] **AND MIRCO IMLAU**[1,*]

[1] *School of Physics, Osnabrueck University, Barbarastrasse 7, 49076 Osnabrueck, Germany*
[2] *Laser Zentrum Hannover e.V., Hollerithallee 8, 30419 Hannover, Germany*
[3] *Wigner Research Centre for Physics, Institute for Solid State Physics and Optics, Hungarian Academy of Sciences, Konkoly-Thege u. 29-33, 1121 Budapest, Hungary*
[*] *mimlau@uos.de*

Abstract: Femtosecond-pulse-induced (E_{pump} = 2.5 eV) picosecond infrared absorption is studied in the spectral region between 0.30 eV and 1.05 eV in LiNbO$_3$:Mg. We find a non-instantaneous mid-infrared absorption peak in the time domain up to 1 ps and a broad-band, long-lived absorption (maximum at 0.85 eV, width $\approx$ 0.5 eV), for $t > 1$ ps. The modelling succeeds by considering small Nb$_{Nb}^{4+}$ electron polaron formation along the sequence: (i) two-photon injection of hot electron-hole pairs at Nb-O-octahedra, (ii) dissociation and electron cooling by electron-phonon-scattering, and (iii) electron self-localization by strong electron-phonon-coupling.

References and links

1. Y. Furukawa, K. Kitamura, A. Alexandrovski, R. K. Route, M. M. Fejer, and G. Foulon, "Green-induced infrared absorption in MgO doped LiNbO$_3$," Appl. Phys. Lett. **78**, 1970–1972 (2001).
2. J. Hirohashi, V. Pasiskevicius, S. Wang, and F. Laurell, "Picosecond blue-light-induced infrared absorption in single-domain and periodically poled ferroelectrics," J. Appl. Phys. **101**, 033105 (2007).
3. S. Favre, T. Sidler, and R.-P. Salathe, "High-power long-pulse second harmonic generation and optical damage with free-running Nd: YAG laser," IEEE J. Quantum Electron. **39**, 733–740 (2003).
4. R. M. Wood, *Laser-Induced Damage of Optical Materials (Series in Optics and Optoelectronics)* (CRC Press, 2003).
5. G. Li and X. Xu, "Thermally induced dephasing of high power second harmonic generation in MgO:LiNbO$_3$ waveguides," Chin. Opt. Lett. **9**, 121901–121904 (2011).
6. O. F. Schirmer, "O$^-$ bound small polarons in oxide materials," J. Phys. Conden. Matter **18**, R667–R704 (2006).
7. O. F. Schirmer, M. Imlau, C. Merschjann, and B. Schoke, "Electron small polarons and bipolarons in LiNbO$_3$," J. Phys. Conden. Matter **21**, 123201 (2009).
8. D. Emin, "Optical properties of large and small polarons and bipolarons," Phys. Rev. B **48**, 13691–13702 (1993).
9. Y. Qiu, K. B. Ucer, and R. T. Williams, "Formation time of a small electron polaron in LiNbO$_3$: Measurements and interpretation," Phys. Status Solidi C **2**, 232–235 (2005).
10. T. Holstein, "Studies of polaron motion," Annals Phys. **8**, 343–389 (1959).
11. D. Berben, K. Buse, S. Wevering, P. Herth, M. Imlau, and T. Woike, "Lifetime of small polarons in iron-doped lithium–niobate crystals," J. Appl. Phys. **87**, 1034–1041 (2000).
12. O. Beyer, D. Maxein, T. Woike, and K. Buse, "Generation of small bound polarons in lithium niobate crystals on the subpicosecond time scale," Appl. Phys. B **83**, 527–530 (2006).
13. D. A. Bryan, R. Gerson, and H. E. Tomaschke, "Increased optical damage resistance in lithium niobate," Appl. Phys. Lett. **44**, 847 (1984).
14. D. Conradi, C. Merschjann, B. Schoke, M. Imlau, G. Corradi, and K. Polgár, "Influence of Mg doping on the behaviour of polaronic light-induced absorption in LiNbO$_3$," Phys. Status Solidi RRL **2**, 284–286 (2008).
15. S. Sasamoto, J. Hirohashi, and S. Ashihara, "Polaron Dynamics in Lithium Niobate upon Femtosecond Pulse Irradiation: Influence of Magnesium Doping and Stoichiometry Control," J. Appl. Phys. **105**, 083102 (2009).
16. S. Enomoto and S. Ashihara, "Comparative study on light-induced absorption between MgO:LiNbO3 and MgO:LiTaO3," J. Appl. Phys. **110**, 063111 (2011).

17. G. M. Greetham, P. Burgos, Q. Cao, I. P. Clark, P. S. Codd, R. C. Farrow, M. W. George, M. Kogimtzis, P. Matousek, A. W. Parker, M. R. Pollard, D. A. Robinson, Z. Xin, and M. Towrie, "Ultra: A unique instrument for time-resolved spectroscopy," Appl. Spectrosc. **64**, 1311–1319 (2010).
18. F. Xin, Z. Zhai, X. Wang, Y. Kong, J. Xu, and G. Zhang, "Threshold behavior of the einstein oscillator, electron-phonon interaction, band-edge absorption, and small hole polarons in linbo$_3$:mg crystals," Phys. Rev. B **86**, 165132 (2012).
19. O. Beyer, D. Maxein, K. Buse, B. Sturman, H. T. Hsieh, and D. Psaltis, "Investigation of nonlinear absorption processes with femtosecond light pulses in lithium niobate crystals," Phys. Rev. E **71** (2005).
20. D. Maxein, S. Kratz, P. Reckenthaeler, J. Bückers, D. Haertle, T. Woike, and K. Buse, "Polarons in magnesium-doped lithium niobate crystals induced by femtosecond light pulses," Appl. Phys. B **92**, 543–547 (2008).
21. X. Yang, G. Xu, H. Li, J. Zhu, and X. Wang, "Optical absorption edge of Mg + Zn: LiNbO$_3$," Cryst. Res. Technol. **31**, 521–527 (1996).
22. T. Roth and R. Laenen, "Absorption of free carriers in diamond determined from the visible to the mid-infrared by femtosecond two-photon absorption spectroscopy," Opt. Commun. **189**, 289–296 (2001).
23. R. Williams and K. Song, "The self-trapped exciton," J. Phys. Chem. Solids **51**, 679–716 (1990).
24. M. D. Fontana and P. Bourson, "Microstructure and defects probed by raman spectroscopy in lithium niobate crystals and devices," Appl. Phys. Rev. **2**, 040602 (2015).
25. G. Blasse, "Fluorescence of niobium-activated antimonates and an empirical criterion for the occurrence of luminescence," J. Chem. Phys. **48**, 3108–3114 (1968).
26. C. Fischer, M. Wöhlecke, T. Volk, and N. Rubinina, "Influence of the damage resistant impurities Zn and Mg on the UV-excited luminescence in LiNbO$_3$," Phys. Status Solidi (a) **137**, 247–255 (1993).
27. D. Emin, "Dynamics of the optically induced properties of a small-polaronic glass," J. Non-Cryst. Solids **35-36**, 969–973 (1980).
28. D. Emin, *Polarons* (Cambridge University Press, 2013).
29. H. Badorreck, S. Nolte, F. Freytag, P. Bäune, V. Dieckmann, and M. Imlau, "Scanning nonlinear absorption in lithium niobate over the time regime of small polaron formation," Opt. Mater. Express **5**, 2729 (2015).
30. M. Imlau, H. Badorreck, and C. Merschjann, "Optical nonlinearities of small polarons in lithium niobate," Appl. Phys. Rev. **2**, 040606 (2015).
31. B. Faust, H. Müller, and O. F. Schirmer, "Free small polarons in LiNbO$_3$," Ferroelectrics. **153**, 297–302 (1994).
32. G. Kitaeva, K. Kuznetsov, V. Morozova, I. Naumova, A. Penin, A. Shepelev, A. Viskovatich, and D. Zhigunov, "Reduction-induced polarons and optical response of Mg-doped LiNbO$_3$ crystals," Appl. Phys. B **78**, 759–764 (2004).

1. Introduction

Pulse-induced transient absorption (TA) is a widely accepted nonlinear optical phenomenon in lithium niobate, LiNbO$_3$ (LN), prominently observed as green- or blue-induced infrared absorption (GRIIRA and BLIIRA) with a relaxation time of several seconds [1, 2]. Due to a long-lived transient absorption, propagating laser pulses in lithium niobate foster to a great extent the appearance of laser-induced bulk- and surface damages, and limits the conversion efficiency mainly by damping [3, 4]. It may also cause phase-detuning via localized crystal heating and the thermo-optical effect [5]. In LN, pulse-induced TA is closely connected with the optical generation of small polarons of the hole and electron type, trapped at O^{2-} and $Nb^{5+}_{Nb/Li}$ sites and absorbing in the blue and near-IR region, respectively [6, 7]. Consequently, the amplitude of the absorption maximum is expected to become proportional to the small polaron number density and the TA spectrum should be determined by the broad-bandwidth optical absorption features of small polarons [8]. The temporal evolution of TA is expected to reflect the complex path of carrier cooling and self-localization via phonon-scattering and -coupling [9], subsequent small polaron transport via thermally activated hopping [10] and its termination, e.g., via electron-hole recombination [11]. As a result, TA in LN ranges over 15 decades of time from sub-picoseconds up to seconds [12] and is best studied by a combination of ultrafast pump-probe spectroscopy (fs - ns) and conventional spectrophotometric techniques (ns - D.C.).

The effects of GRIIRA/BLIIRA can almost completely be suppressed by doping LN with Mg, Zn, etc. over their respective threshold concentrations [1]. The doping has the effect to eliminate Nb^{5+}_{Li} antisite defects in LN and, thus, suppresses the formation of Nb^{4+}_{Li} electron and $Nb^{4+}_{Li}:Nb^{4+}_{Nb}$ (bi-)polarons. Although the optical damage resistance is fairly increased in the visible range [13] a significant TA in the visible as well as in the infrared spectral region at timescales $< 10^{-5}$ s becomes more dominant in Mg-doped LN [14]. Despite the broad knowledge on the

dependence of GRIIRA/BLIIRA on the crystal composition only little is known about the spectral and temporal properties of TA. In particular, nearly nothing is known about the TA in the mid-IR (MIR) on the ultrafast time scale which is mandatory for the further improvement of high-power mid-infrared optical parametric oscillators (OPOs).

This contribution focuses on the spectral detection of picosecond MIR-TA in LN:Mg related to small Nb_{Nb}^{4+} free polaron (FP) formation in the range between 0.30 eV and 1.05 eV that is difficult to access from the experimental point of view. Our study uncovers that free polaron TA is overlaid by a non-instantaneous, broad-band MIR absorption peak on timescales up to ≈ 1 ps that cannot be attributed to multi-photon absorption processes. Under the assumption of pulse-injection of hot-electron-hole pairs, electron-phonon-scattering and -coupling, both TA contributions can well be separated on the temporal axis. An undisturbed, broad-band small polaron absorption spectrum emerges at a temporal delay of 2 ps after the pump pulse. The obtained data set can be quantitatively modelled on the basis of theoretical expectations for the formation and absorption of small, free Nb_{Nb}^{4+} polarons tested earlier using steady-state spectrophotometric techniques in thermally pre-treated Mg-doped LN and TA-measurements limited to near-IR frequencies [9, 15, 16].

2. Experiment

2.1. VIS-pump-MIR-probe spectrometer

The ps-MIR TA studies were performed by a home-made VIS-pump-MIR-probe spectrometer (schematically sketched in the insert of Fig. 1, for a typical setup see [17]) with a temporal resolution $\Delta t \approx 200$ fs, beam diameters of $d_{pump} = (500 \pm 50)$ μm, $d_{probe} = (400 \pm 50)$ μm and an intersection angle of $\alpha = (8 \pm 1)°$. The pump (2.5 eV; $\tau_{pump} = (100 \pm 10)$ fs; I_{pump}^0 up to 2.5 PW $\cdot$ m^{-2}; $f_{pump} = 500$ Hz) and the probe (0.30 eV - 1.05 eV; $\tau_{probe} \approx 170$ fs; $I_{probe}^0 < 0.03$ PW $\cdot$ m^{-2}, $f_{probe} = 1$ kHz) pulses are polarized along the c-axis and within the plane of the incident pulses. The infrared signal was detected with a spectral resolution of $\Delta\omega/\omega < 10^{-3}$ and a sensitivity $\Delta\alpha/\alpha \approx 2 \cdot 10^{-2}$ (exemplarily at 0.6 eV) using a combination of a Czerny-Turner spectrograph and a mercury-cadmium-telluride-detector pixel array (32-elements). To improve the signal to noise ratio, every data point is averaged over 2000 sequential pump-probe events. A single crystal (dimensions 6×7 mm^2; thickness (200 ± 10) μm) of near-stoichiometric LiNbO$_3$:Mg (Mg concentration in the melt 1.0 mol, residual iron content below 5 ppm, estimated molar Li/Nb ratio in the crystal 0.985), grown at the *WIGNER Research Centre for Physics*, Budapest, Hungary is used with a fundamental absorption in the near- to mid-infrared spectral range not exceeding $\alpha_0 = 100$ m^{-1} over the spectral range under investigation (0.30 eV$-$1.05 eV), apart from absorption due to OH$^-$-stretching vibrations in the spectral window $E = (0.424 - 0.443)$ eV [13]. The exact time of maximum overlap between pump and probe pulses was determined using the signal generated via difference frequency generation (DFG) in the LN sample under study (photon energy at about 2 eV). The DFG process was enabled by a weak phase-matching condition using a very thin sample as well as a slightly non-collinear geometry (outer angle $\alpha = (8 \pm 1)°$ between the incident pulses). The DFG pulse energy was measured by a standard Si-detector in transmission geometry. The temporal profile of the DFG signal was measured individually for each probe photon energy. Slight differences in the tails of the qualitatively similar profiles were observed and attributed to differences in the probe pulse durations. The two-photon absorption coefficient is determined to $\beta = (7.9 \pm 0.3)$ mm $\cdot$ GW^{-1} at 2.5 eV. Laser-induced damages of surface and bulk as well as cumulative effects of the MIR-TA between two sequential pump events were carefully checked, but not observed for $I_{pump}^0 = 1.4$ PW $\cdot$ m^{-2}.
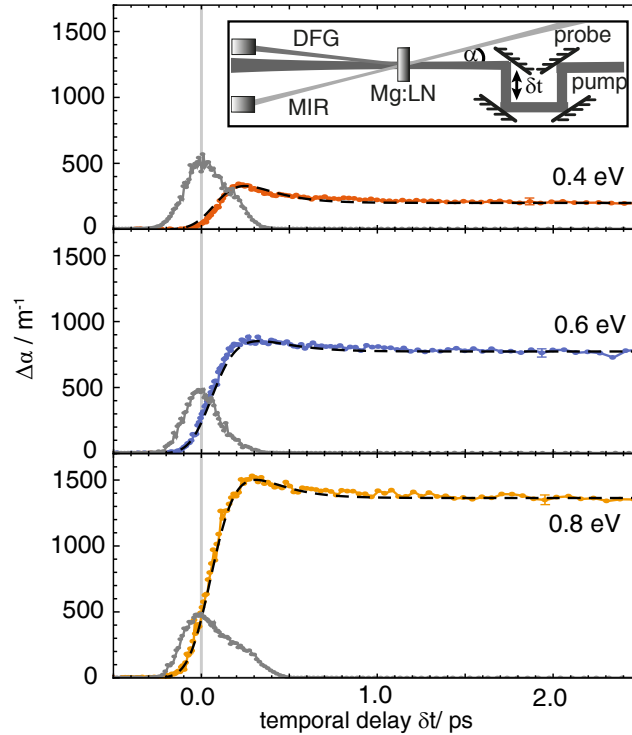
Fig. 1. Transient absorption in the ps range for a 2.5 eV pump pulse (I^0_{pump} = $(1.4 \pm 0.2)\,\text{PW/m}^2$) and probe photon energies E_{probe} = 0.40 eV (3000 nm), 0.60 eV (2066 nm), 0.80 eV (1550 nm). The transient absorption is defined as $\Delta\alpha(E_{\text{probe}}, \delta t) = \alpha(E_{\text{probe}}, \delta t)_{\text{pumped}} - \alpha(E_{\text{probe}}, \delta t)_{\text{unpumped}}$. The depicted values represent the average over 2000 pump-probe events and the error margin is given by the standard deviation. The gray data points are the corresponding DFG correlation signal between pump and probe pulse (schematic setup shown in the insert) and the dotted black lines correspond to the numerical fits (see chapter 3.2).

2.2. Transient absorption of LN:Mg in the infrared spectral range

Figure 1 shows the transient absorption $\Delta\alpha(\delta t)$ of LN:Mg for three probe photon energies (E_{probe} = 0.4 eV, 0.6 eV, and 0.8 eV) as examples. The vertical gray line (cf. Fig. 1) marks the zero point δt = 0 defined as the maximum of DFG between pump and probe pulses (type-II eoe phasematching). The cross-correlation signal (dark gray dots in Fig. 1) has a Full-Width-Half-Maximum (FWHM) of $(200 \pm 10)\,\text{fs}$.

All transients of Fig. 1 show qualitatively similar TA dynamics: A moderate non-instantaneous absorption peak dominates the time domain up to 1 ps after the pump pulse. Its maximum shows a marked dependence on the photon energy of the probe pulse and increases from $\Delta\alpha^{\text{max}} \approx 340\,\text{m}^{-1}$ (0.4 eV) up to $\Delta\alpha^{\text{max}} \approx 1520\,\text{m}^{-1}$ (0.8 eV). It is important to note that this absorption peak has a remarkable temporal shift of $\Delta t^{\text{peak}} \approx (270 \pm 30)\,\text{fs}$ (0.6 eV) compared to the pump pulse. In the time domain $t > 1$ ps, a plateau absorption materializes with an amplitude that also depends on the photon energy. The values, e.g., at $\delta t = 2.5$ ps, rise from $\Delta\alpha(2.5\,\text{ps}) = (200 \pm 10)\,\text{m}^{-1}$ (0.4 eV) up to $\Delta\alpha(2.5\,\text{ps}) = (1350 \pm 20)\,\text{m}^{-1}$ (0.8 eV) and remain constant all over the sub-ns time domain. Similar data sets were obtained for all probe photon energies in the investigated range between 0.30 eV and 1.05 eV. For photon energies below 0.4 eV as well as those above

0.8 eV, the MIR-TA shows a clear tendency to smaller values of $\Delta\alpha^{\mathrm{max}}$ and $\Delta\alpha(2.5\,\mathrm{ps})$. All transients were investigated as a function of pump peak energy in the range from $0.03\,\mathrm{PW/m^2}$ to $2.50\,\mathrm{PW/m^2}$ and for different polarizations, as well. Qualitatively, the transients show a similar behavior, but the overall absorption change rises with increasing peak energy. In particular, a quadratic dependence of non-instantaneous peak maximum and plateau absorption is found. The polarization of the beams was chosen to optimize the absorption signal (in accordance with Ref. [15]).

Similar transients were obtained for different crystals of the same boule. We have limited our study to a Mg concentration in the melt of 1.0 mol% in order to suppress the impact of either Nb_{Li}^{4+} formation (for lower Mg concentrations) and of the incorporation of Mg on Nb sites (larger Mg concentrations) [18]. Furthermore, only slight differences in the observed time constants and absolute values of the absorption signals are to be expected (cf. Ref. [15]).

3. Discussion

3.1. Carrier-formation path

These data cannot be explained straightforwardly with the state-of-the-art knowledge of picosecond TA in LN and provide further insights into the optical formation of small Nb_{Nb}^{4+} electron polarons. In particular, to our knowledge, there are no reports on a temporal shift of the absorption peak of the TA with respect to the incident pump pulse in LN for any probe energy. This observation most likely remained inaccessible since the zero point $\delta t = 0$ has been assigned to the time of the maximum value of the absorption peak in recent studies. Consequently, the absorption peak itself was attributed to a *quasi-instantaneous* non-linearity, i.e., non-degenerate two- or multi-photon absorption in Refs. [15, 19, 20] using probe energies E_{probe}=1.55 eV in nominally undoped LN and LN:Mg. For the given fs-pump-probe technique some delay between the pump and a non-degenerate Two-Photon-Absorption (TPA) peak might indeed be expected due to the different group velocities of the probe and pump pulse, as it has been discussed comprehensively by Beyer et al. [19]. According to our experimental approach, we here need to consider the GVD difference between the probe and the DFG pulses. For this case, our calculations reveal temporal corrections of up to $\delta t = (50 \pm 10)\,\mathrm{fs}$ depending on the probe photon energy. These values are below our temporal resolution ($\approx 200\,\mathrm{fs}$) and below the discovered temporal offset between DFG maximum and non-instantaneous absorption peak. The temporal offset can therefore not be attributed to the effect of GVD, only. Furthermore, the probe photon energies between 0.30 eV and 1.05 eV of our experiment are insufficient to enable non-degenerate two-photon absorption with a pump photon energy of 2.5 eV at a band gap energy of LN of $\approx 3.92\,\mathrm{eV}$ [21]. Three-photon interaction of two VIS and one MIR photons may be assumed, instead, but this does not comply with the considerable TA signal amplitudes of our study. However a similar shift of the peak-absorption, dependent on the photon energy, has been reported for diamond [22]. The authors attribute this phenomenon to the long-lasting presence of electrons within the conduction band.

In what follows, we attribute our findings to small Nb_{Nb}^{4+} electron polaron formation according to the process schematically depicted in Fig. 2.

It is reasonable to expect the excitation of hot electron-hole pairs (hot excitons) to occur in a process localized within a Nb-O-octahedron of the LN structure. Such e^--h^+-pairs may recombine immediately (1) or may become self-trapped as self-trapped excitons (STE) [23] by strong coupling to the lattice (2). According to the phonon frequencies in LN up to the 10 THz range [24], the latter process will be delayed by a few hundreds of femtoseconds. It is noteworthy that the STE decay is closely connected with the emission of light in the blue-green spectrum in Mg-doped LN crystals [25, 26] as used in our present study. Path (3) marks the possibility of phonon-assisted small polaron formation from an essentially unrelaxed e^--h^+-pair [27] by transfer of the electron to a next-neighboring Nb_{Nb}^{5+} ion (analogously, a transfer of a hole to a next
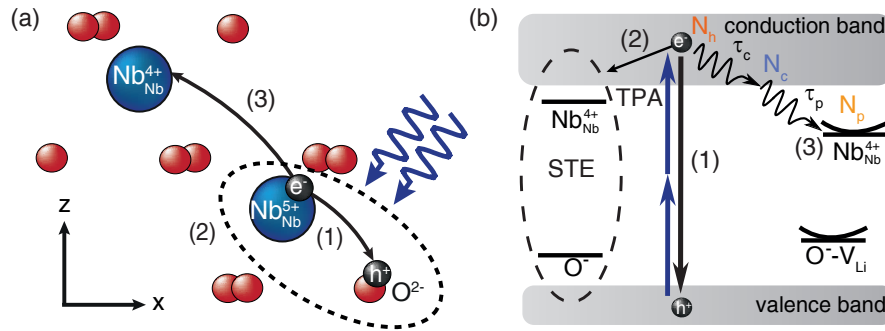
Fig. 2. Recombination paths of fs-pulse generated hot electrons and holes in LN:Mg displayed (a) in a model of the atomic structure and (b) in an energy level diagram. Three recombination paths are considered: (1) the direct recombination of electrons and holes, (2) the formation of self-trapped excitons within a Nb-O-octahedron, and (3) the phonon-assisted formation of small polarons. Our modelling of Eqs. 1-3 is based on relaxation path (3), i.e., paths (1) and (2) are disregarded in our model. This assumption accords with our experimental setup and crystal choice being tailored for small free polaron detection. Furthermore, it considers the comparably low probability for paths (1) and (2).

neighboring O^{2-} also resulting in the dissociation of the $e^- \text{-} h^+$-pair may also be considered). This electron will be cooled by means of electron-phonon scattering prior to self-localization via electron-phonon coupling. From the perspective of our experiment, we will be able to detect the MIR absorption features of cooled electrons and Nb_{Nb}^{4+} electron polarons. In contrast, hot exciton states, that most probably show a UV/blue absorption feature, may not be accessible within the spectral region of our probe pulse. As a result, the transients in the MIR should reflect at least two main characteristic time constants: τ_c that takes into account the phonon-assisted processes of $e^- \text{-} h^+$ dissociation and hot-electron cooling and τ_p that is determined by the response time of the lattice.

A very similar understanding of TA related to small free Nb_{Nb}^{4+} polaron formation in MgO-doped LN was presented by Qiu et al. [9]. Although a non-instantaneous absorption peak of TPA was not observed, after a delay of the order of 1 ps a long-lived absorption plateau with rise time of about 200 fs at room temperature was clearly discovered and attributed to the formation of Nb_{Nb}^{4+} polarons. The delay was assigned to phonon-assisted cooling of optically excited hot carriers and the time required for carrier localization by electron-phonon coupling. We here note, that paths (1-3) represent three different options for the initially generated electron hole pair. According to D. Emin [28] a sequence of paths (2) → (3) may occur, i.e., the transformation of a STE into a Nb_{Nb}^{4+} electron and O^- hole polaron. In our modelling, however, we disregard paths (1) and (2) as well as a sequential formation process due to a low probability for these processes. In agreement with a theoretical estimate, a delay time of about 80 fs [9] was deduced for the cooling process. In a recent work of Badorreck et al. [29], we were able to verify this delay-time experimentally in nominally undoped, congruent LN with a value of $\tau_c \approx 80$ fs for a TPA excitation process at 2.5 eV, i.e., equivalent to this work.

The characteristics of the absorption plateau remain in full accordance with the state-of-the-art knowledge on TA in the near-infrared spectral range. Its interpretation via small, strong-coupling Nb_{Nb}^{4+} electron polarons is verified by a temperature dependent formation time of a few hundred femtoseconds [9, 15, 19, 20]. The respective decay process obeys a stretched-exponential behavior with a decay time in the regime of a few hundred nanoseconds (over-threshold LN:Mg) [14, 15, 20]. This is short enough to avoid cumulative effects upon repetitive polaron formation at frequencies of 1 kHz.

3.2. Modelling

Based on these considerations, we will now turn to the numerical analysis of our data applying the following set of rate equations:

$$\frac{\partial N_h(L,t)}{\partial t} = \frac{\beta I^2(L,t)}{2\hbar\omega} - \frac{N_h(L,t)}{\tau_c} \tag{1}$$

$$\frac{\partial N_c(L,t)}{\partial t} = \frac{N_h(L,t)}{\tau_c} - \frac{N_c(L,t)}{\tau_p} \tag{2}$$

$$\frac{\partial N_p(L,t)}{\partial t} = \frac{N_c(L,t)}{\tau_p}, \tag{3}$$

where L is a coordinate along the light propagation direction in the crystal, β the TPA-coefficient at the photon energy of the pump pulse $\hbar\omega$, $N_{h,c,p}$ the number densities of injected hot electrons, cold electrons, and polarons, respectively and $I(L,t)$ is the pump light intensity inside the crystal for a gaussian shaped pulse influenced by two-photon absorption based on the considerations from Beyer et al. [19]:

$$I(t,L) = \frac{2 \cdot \exp[-4\log(2)(\frac{t}{\tau_{pump}})^2]}{\beta L \sqrt{\pi}} \int_0^\infty \ln[1 + \beta I_{pump}^0 L \cdot \exp(-s^2)]\, ds. \tag{4}$$

The calculated transient absorption signal α_{calc} is given by the mean value over the sample length d of the sum of three individual number densities multiplied by their respective absorption cross sections:

$$\alpha_{calc}(t) = \frac{1}{d} \int_0^d [\sigma_p \cdot N_p(L,t) + \sigma_h \cdot N_h(L,t) + \sigma_c \cdot N_c(L,t)]\, dL. \tag{5}$$

For comparison with the experimentally determined transient absorption α_{exp} the calculated absorption α_{calc} has to be convolved with the gaussian temporal envelope of the probe pulse:

$$\alpha_{exp}(\Delta t) = 2\sqrt{\frac{\log(2)}{\pi\tau_{probe}^2}} \int_{-\infty}^\infty \alpha_{calc}(t) \cdot \exp\left[-4\log(2)\left(\frac{t-\Delta t}{\tau_{probe}}\right)^2\right]\, dt \tag{6}$$

This interplay of three types of carriers (see Eq. 5) is the key for a successful modelling of the determined characteristics of the MIR-TA. The numerical solution of equations (1)-(6) with the simultaneous fitting of the parameters $\tau_{c,p}$ and $\sigma_{h,c,p}$ could only be performed with the following restrictions: (i) at $t = -300\,\text{fs}$ the number densities of all carriers are assumed to be zero, (ii) according to the sequence of carriers in our approach the number densities initially have to fulfill the relation $N_h^{total} \geq N_c^{total} \geq N_p^{total}$, (iii) the absorption cross section of hot electrons in the MIR is neglected: $\sigma_h \approx 0$, and (iv) electronic cooling stages are faster than lattice relaxation (both on the sub-ps scale): $\tau_c < \tau_p \ll 1\,\text{ps}$. Again, we note that losses of the probe pulse by three-photon absorption including the pump pulse are not considered.

Figure 3 compares the spatially integrated, convolved outcome of fitting equation (6) (green line) to the experimental data set (green dots), exemplarily for $E_{probe} = 0.6\,\text{eV}$.

The temporal evolution of the individual number densities $N_h(t)$, $N_c(t)$ and $N_p(t)$ at $L = 200\,\mu\text{m}$ are depicted as determined from the solution of the rate equations (1)-(3). Fitting was performed for all spectra with a very high quality according to the fitting results depicted as dotted lines in Fig. 1 (normalized root-mean-square deviation (NRMSD) values of (7.1% (0.4 eV), 3.0%
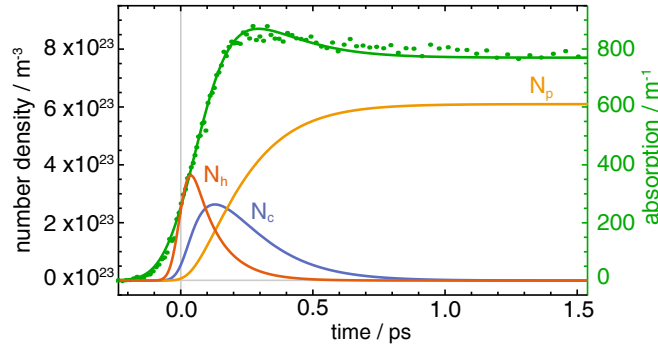
Fig. 3. Numerical fit of the transient absorption (green line) and the data set (green dots) at 0.6 eV. Fitting parameters: τ_c = 100 fs and τ_p = 150 fs. The dynamics of the individual number densities are calculated assuming full conversion of pump photons to hot electrons and are plotted as orange (N_h), blue (N_c) and yellow (N_p) lines. Note that N_h does not contribute to the MIR absorption as σ_h = 0, but is still fully defined due to the nonlinear term in Eq. 1.

(0.6 eV), 2.3% (0.8 eV)). We note that the fitting procedure was performed iteratively for all photon energies using the same set of free fitting parameters τ_c = 100 fs, τ_p = 150 fs.

All fitting parameters agree very well with previously reported values of the generation time of free ($\approx$ 100 fs in [15]) and bound polarons ($<$ 400 fs in [12], [30]) and the free electron cooling time (cf. $\tau_c \approx$ 80 fs in [9, 29]), confirming our assumptions. We note, that the sum of τ_c and τ_p may be interpreted as polaron formation time with respect to the incident pump pulse.

In the time range of -0.2 ps$< t < 1$ ps, we find that only the number densities of cold electrons and polarons contribute to the overall TA signal. For $t > 1$ ps, on the other hand, TA is solely determined by the absorption of small, strong-coupling polarons. At the same time, our fit reveals a non-zero population of hot carriers at the maximum of the incident pulse. This feature can be attributed to the temporal width of the incident pulse peak with a pulse duration of $\approx$ 100 fs at peak maximum $t = 0$ fs. Therefore, it must be considered that the pump pulse intensity already rises considerably at $t \approx -50$ fs that results in a non-zero population of hot carriers at $t = 0$ fs.

3.3. Small polaron fingerprint

Based on these findings, it is possible to deduce the absorption fingerprint of Nb_{Nb}^{4+} electron polarons by plotting the spectral dependence of the TA signal at a fixed delay time of $t = 2$ ps as displayed in Fig. 4.

The data reveal a broad spectral distribution with a maximum at $E(h\nu)_{peak} \approx 0.80$ eV that can be applied for an estimate of the small-polaron stabilization energy E_p due to the induced lattice distortion: $E_p = (1/2)E(h\nu)_{peak} \approx 0.40$ eV. A more precise approach with respect to the asymmetric shape of the spectral distribution is given by Emin's theory of small free polarons at elevated temperatures [8]:

$$\Delta\alpha(\hbar\omega) \propto \frac{1}{\hbar\omega} \exp[-(2E_p - \hbar\omega)^2/(8E_p k_B T)], \qquad (7)$$

describing the lineshape in excellent agreement with experimental data (cf. solid line in Fig. 4), with k_B being the Boltzmann constant. The fit yields the free polaron binding energy $E_p = (0.44 \pm 0.02)$ eV, a peak maximum at $E(h\nu)_{peak} = (0.83 \pm 0.04)$ eV and a half width at half maximum of $W = (0.26 \pm 0.01)$ eV at room temperature and $t = 2$ ps. A comparison of the values obtained in this study with previous investigations using thermally stabilized small polarons
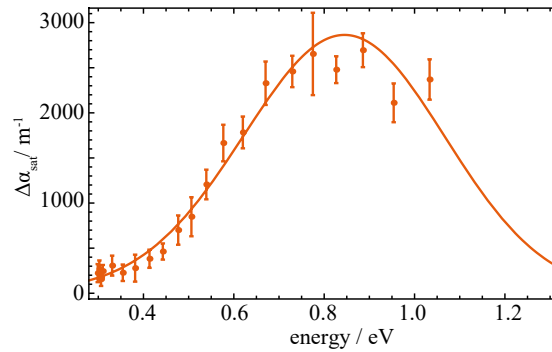
Fig. 4. Absorption fingerprint of fs-pulse induced free polarons at a fixed time delay of $t = 2\,\text{ps}$ ($I^0_{\text{pump}} = (2.5 \pm 0.2)\,\text{PW/m}^2$). The continuous line fits Eq. 7 to the experimental data set. The error margin is given by the standard deviation and the error made by determining the light intensity.

is given in Tab. 1. The peak position is in agreement with previous studies, whereas slight differences can be seen in the case of the spectral width.

The discovered differences can be attributed to (i) the use of an asymmetric fitting function and (ii) the impact of a non-equilibrium electronic state that has to be expected on the picosecond time scale after exposure to an intense fs-laser pulse. Driving evidence for the latter conclusion is the short lifetime of a few μs of the transient absorption with a complete recovery of the involved electronic state.

Table 1. Polaron stabilization energy E_p and half width at half maximum W of the MIR absorption feature in comparison.

E_p(eV)	W(eV)	T(K)	Reference
0.44± 0.02	0.26 ± 0.01	295	this study
0.48	≈ 0.23	295	[31]
0.54	≈ 0.40	6	[31]
0.54	0.37	295	[7]
0.47	≈0.25	295	[32]

4. Conclusion & novelty

In conclusion, our analysis clarifies the picosecond transient absorption of femtosecond-pulse injected carriers during their relaxation to small free $\text{Nb}^{4+}_{\text{Nb}}$ electron polarons in the spectral range of 0.30 eV up to 1.05 eV. It extends the knowledge about the optical properties of small electron polarons to the ultrafast time regime that also comprises small polaron formation.

From a fundamental viewpoint, our findings demonstrate that the theoretical concepts about the optical properties of small, strong-coupling polarons (Holstein-Emin approach) can be transferred to the field of nonlinear optics and femtophysics in general, i.e., to the non-equilibrium state, which is indicated by a fair agreement of the spectral parameters of the TA plateau with 'steady-state' values for free polarons.

A specific result of our study is the interpretation of the TA maximum as a non-instantaneous absorption peak due to an intermediary (unrelaxed cold) electron state that cannot be attributed to the action of multiphoton absorption. This was obtained using a methodical peculiarity of fs-VIS-pump-MIR-probe spectroscopy in nonlinear optical LN that makes use of the difference frequency generation signal between pump and probe to define the exact time of maximal overlap.

By comprehensive modelling of the multi-step flow of electronic energy induced by two-photon absorption, that was missing in the literature so far, existing models for small polaron formation are supported, confirming also predictions for the lifetimes of early stages despite the negligible mid-IR absorption of hot electrons. The ps-MIR TA may be considered for fs-pulse-exposed frequency converters based on lithium niobate crystals and for the further development and engineering of demanding high-power MIR fs-laser sources using polar representatives of niobates and of the borate class (LBO, BBO, etc.).

This study may also serve as a hint for the need of a further subdivision of the small polaron formation process and will push forward studies on the appearance and transport of hot excitons by probing the UV/VIS spectral range.

Funding

Acknowledgements